Materials Today Advances 30 (2026) 100773

Contents lists available at ScienceDirect

Materials Today Advances

journal homepage: www.journals.elsevier.com/materials-today-advances/

Bioelectronic skin-conducting polymer interface: Assessing the role of nanopores and appendages

Povilas Virbickas [a,b,c,d,*], Sebastian Björklund [a,b], Skaidre Jankovskaja [a,b], Emelie Nilsson [a,b], Aušra Valiūnienė [c,d], Johan Engblom [a,b], Tautgirdas Ruzgas [a,b]

[a] Department of Biomedical Science, Faculty of Health and Society, Malmö University, Malmö, Sweden
[b] Biofilms Research Centre for Biointerfaces, Malmö University, Malmö, Sweden
[c] Faculty of Chemistry and Geosciences, Vilnius University, Vilnius, Lithuania
[d] State Research Institute Center for Physical Sciences and Technology, Vilnius, Lithuania

ARTICLE INFO

Keywords:
Skin
Electrochemical impedance spectroscopy
Polypyrrole
Conducting polymer
Nanopores
Bioelectronics

ABSTRACT

The integration of biological tissues with conducting polymers is crucial for the advancement of bioelectronics. Although the potential toxicity of some conducting-ink components is an acknowledged constraint for *in vivo* use, a more fundamental limitation is the lack of molecular understanding of how conducting polymers interact with biological barriers. This study addresses some of the limitations by presenting a novel method for direct polymerization of pyrrole on excised skin *in vitro* and investigates the evolving skin/conducting polymer interface using electrical impedance spectroscopy (EIS), X-ray diffraction, vapor sorption, and complementary analyses. Direct polymerization of pyrrole on skin is performed by applying an aqueous pyrrole solution to the dermal side and an oxidant (ferric ion solution) on the stratum corneum (SC) side of the skin membrane fixed in a Franz cell. EIS measurements show a marked reduction in skin barrier resistance after PPy formation, whereas control experiments produced the opposite trend, confirming that the resistance drop arises specifically from polymerization. Our complementary analyses indicate that polymerization is primarily localized at the solution-SC interface but also support the formation of an electrically coupled pathway across the barrier. These results provide molecular-level insight into polymer-SC interactions, imply the formation of a coherent conductive junction that extends through the SC layers, and inform the design of future skin-integrated bioelectronic materials.

1. Introduction

The integration of biological and electronic systems in bioelectronics is driving advances in medical technology, particularly in diagnostics and therapy. Establishing a seamless interface between electronics and skin is a critical area of research. In diagnostics, biosensors in wearable or semi-implantable devices on the skin offer a promising approach, enabling continuous real-time monitoring of health metrics and early detection of disease [1,2]. In therapeutic applications, the interface between electronics and the skin can be leveraged for improved and controlled transdermal drug delivery [3]. Techniques such as electroporation, which applies high-voltage pulses to create temporary pores in the stratum corneum (SC), and iontophoresis, which uses a low electric current to drive charged drug molecules through the SC, exemplify electrical methods used to enhance drug delivery through the skin [4,5]. Importantly, transdermal drug delivery typically requires enhancing the permeability of the SC [6].

An effective approach to engineering bioelectronic interfaces on the SC can be achieved by using conducting polymers, such as polypyrrole (PPy), poly(3,4-ethylenedioxythiophene) (PEDOT) and polyaniline [7,8]. The polymerization processes occurring within or on the skin barrier remain poorly understood, yet are essential for the development of novel epidermal sensors and topical therapeutic applications. However, the *in vivo* research is restricted due to the toxicity of monomer components of polymerization mixtures. While searching for biocompatible conducting polymer deposition recipes, a good deal of research questions about conducting polymer/skin interaction and bioelectronics interfacing with skin can be addressed by *in vitro* investigations.

This study introduces a novel Franz cell-based method to form networks of conducting organic polymers directly on SC, building on recent

* Corresponding author. Department of Biomedical Science, Faculty of Health and Society, Malmö University, Malmö, Sweden.
E-mail address: povilas.virbickas@mau.se (P. Virbickas).

https://doi.org/10.1016/j.mtadv.2026.100773
Received 31 October 2025; Received in revised form 24 March 2026; Accepted 31 March 2026
Available online 5 April 2026

biosensor applications studies [9]. As a model monomer for developing a skin-conducting polymer interface, pyrrole was chosen due its low molecular weight (67 g mol^{-1}), good solubility in water (45 g l^{-1} [10]), and the ability of PPy to reach conductivities in the mS cm^{-1} range and above when synthesized using $FeCl_3$ [11,12]. Here, we demonstrate for the first time the formation of seamless skin-electrode interfaces using this setup. A pyrrole monomer solution was applied to the dermal side of porcine skin membranes fixed in a Franz cell, while a ferric ion (Fe^{3+}) oxidant solution was placed on the outermost SC side. This pyrrole/skin/Fe^{3+} configuration drove polymerization selectively on the SC. The Franz cell-based *in vitro* approach is proven especially valuable for investigating the polymerization of toxic monomers (e.g., pyrrole or aniline), which is often performed with potentially hazardous oxidants, on skin. It enables characterization of seamless conducting polymer/skin interaction, while searching for biocompatible recipes enabling chemical deposition of bioelectronic systems on humans or animals.

Electrochemical impedance spectroscopy (EIS) was employed to assess the effects of the polymerization process both on skin resistance and effective capacitance. For the first time, it allowed us to observe a manifestation of nanopores through the salt concentration-induced changes in membrane resistance. Small- and wide-angle X-ray diffraction was utilized to investigate changes in the molecular organization of lipids and keratin in the SC due to pyrrole polymerization. Additionally, Fourier transform infrared (FTIR) spectroscopy was used to determine the extent of polymerization on SC *vs* dermal sides of the skin membrane, accounting placement asymmetry of the monomer *vs* the oxidant. These techniques have previously been used to study the effects of hydration and Ultraviolet B radiation (UVB) on the skin [13,14]. The growth of polypyrrole deposits on the skin surface was visually documented using optical microscopy.

The results of this study prove that the proposed Franz cell-based methodology can be adapted to produce and study seamless bioelectronic interfaces created between skin and conducting polymer. This *in vitro* approach can also be further explored on other bio-barrier models, e.g., viable 3D skin, before progressing towards *in vivo* studies on humans or animals.

2. Experimental

2.1. Materials

$FeCl_3{\cdot}3H_2O$, pyrrole (98%), HCl (30%) and phosphate-buffered saline (PBS) tablets were purchased from Sigma-Aldrich (St. Louis, USA). KCl and KH_2PO_4 were obtained from Merck (Darmstadt, Germany). 500 Da cut-off Spectrum™ Spectra/Por™ Biotech cellulose ester dialysis membrane (DM) and aniline (99%) was purchased from Fisher Scientific (Waltham, USA). Deionized water was obtained using Milli Q-plus-Millipore system (Burlington, USA). PBS (pH 7.4, 140 mM of NaCl, 3 mM of KCl, 10 mM of phosphate) was prepared by dissolving PBS tablets in deionized water. Phosphate-buffered KCl solutions of various KCl concentrations (0.2 M − 0.01 M) were prepared by dissolving K_2HPO_4 (1 mM), KCl (concentration between 0.2 M and 0.01 M) in deionized water and adjusting pH to 7.4 with HCl.

2.2. Preparation of porcine skin samples

Porcine ears acquired from a local abattoir and stored at − 80 °C were used to prepare skin membranes. The ears were residuals from food preparation, thus ethical permission for working with them was not required. The skin membranes were prepared as reported earlier [13]. Briefly, defrosted porcine ears were cleaned with cold water and cut into strips, shaved and sliced to obtain approximately 500 μm thick skin membranes using a dermatome (TCM 3000 BL, Nouvag, Konstanz, Germany). The resulting skin samples were punched to obtain circular membranes (ca. 16 mm diameter). The membranes then were kept at − 80 °C on filter paper until they were used.

2.3. Modification of porcine skin samples and dialysis membrane with polypyrrole

Cellulose ester dialysis membranes (DM) and porcine skin membranes were modified with polypyrrole (PPy) by applying Fe^{3+} ions as oxidant agents in the presence of pyrrole monomers [15]. The biocompatibility of PPy has been studied previously, including its influence on keratinocytes and other cell types [16–18]. To perform the polymerization of pyrrole on the membranes, the DM or the skin with the SC upwards were placed in vertical Franz cells. The lower cell compartment was charged with a 0.15 M pyrrole solution in deionized water. The upper cell compartment was charged with 0.06 M $FeCl_3$ solution in water. Considering that skin has higher permeability for small neutral molecules than ions [19–21], this arrangement of solutions promoted polypyrrole polymerization on the top of the skin (SC side, Fig. 1). Deposition of PPy proceeded for 24 h, resulting in PPy-modified skin (PPy-skin) or dialysis membranes (PPy-DM), respectively.

2.4. Electrochemical impedance spectroscopy of membranes

Electrochemical impedance spectroscopy (EIS) was used to evaluate the membranes before and after PPy polymerization (*i.e.*, unmodified and PPy modified). Measurements were conducted in Franz cells filled with PBS or a specified electrolyte solution. Initial impedance measurements were done after membrane equilibration in PBS for 1 h, after which the polymerization of pyrrole was conducted for 24 h. After the polymerization, the solutions in the Franz cell were replaced with fresh PBS to allow for the final EIS measurement (recorded within 30 min). Similar experiments were performed with cellulose membranes, serving as a reference experiment. The EIS measurements were performed in a Franz cell equipped with 4 electrodes [13]. Pt wires were used as working and counter electrodes, while Ag|AgCl (KCl_{sat}) electrodes served as reference and sensing electrodes. EIS spectra were registered using a potentiostat from Ivium Technologies (Eindhoven, Netherlands) in 0.01 Hz - 1 MHz frequency range, and an applied AC voltage amplitude of 20 mV at zero DC voltage. EIS spectra of DM and PPy-DM were registered in PBS. EIS spectra of skin and PPy-skin membranes were registered in PBS or in 1 mM phosphate-buffered solutions (pH 7.4) containing various KCl concentrations in the range from 0.01 M to 0.2 M. The "Zview" was used to fit the data to an equivalent circuit model allowing estimation of solution resistance, membrane resistance and membrane constant phase element.

2.5. Preparation of SC samples

SC samples were obtained by removing the SC layer from PPy-SC and unmodified porcine skin membranes using a trypsin solution (0.2 %) in PBS [13]. Skin membranes were placed on a filter paper soaked in trypsin solution for 12 h at 4 °C. The SC layer was then separated from the trypsin-treated skin using a tweezer, wiped with a cotton swab to remove the underlying tissue, and rinsed with PBS.

Given that EIS measurements of a skin membrane performed in a four-electrode configuration predominantly reflect the properties of the densely packed SC layer (as ionic permeation through skin is primarily restricted by the SC [21–23]) the isolated SC sheets were used in FTIR, DVS, and X-ray diffraction analyses for deeper characterization of its structural changes due to development of PPy-SC interface.

2.6. Preparations of polypyrrole flakes

PPy flakes for FTIR analysis and dynamic vapor sorption studies were prepared by mixing aqueous solutions of pyrrole (0.15 M) and $FeCl_3$ (0.06 M) and allowing the reaction to proceed undisturbed 4 h until PPy flakes precipitated. The resulting PPy flakes were filtered on Whatman®

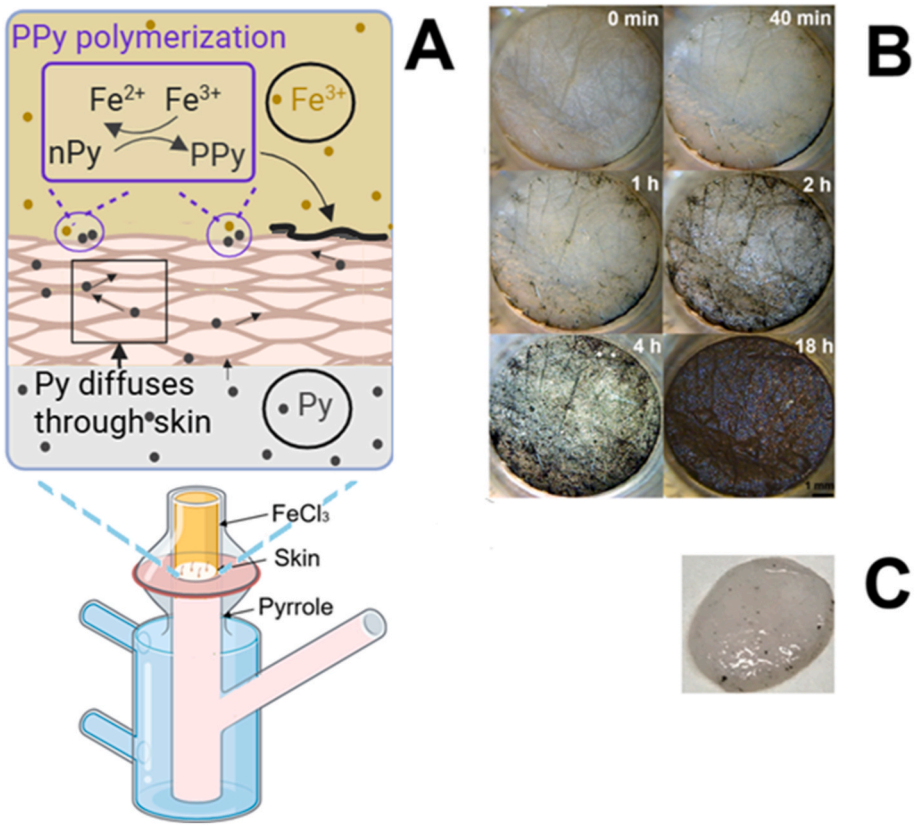

Fig. 1. A - Schematic representation of PPy deposition on the skin surface using a Franz cell setup. Created with BioRender.com (publication license granted to Sebastian Björklund/Malmö University). **B -** photos of a porcine skin taken during its modification with polypyrrole; indicated time from the start of polymerization experiment. **C -** photo of a PPy modified skin membrane after removal of SC by trypsin solution (0.2 % in PBS). Black spots on the skin membrane are residues of SC that remained after the treatment with trypsin.

filter paper (grade 4, from Sigma-Aldrich, St. Louis, USA) and washed 3 times with deionized water.

2.7. Small- and wide-angle X-ray diffraction (SAXD and WAXD)

SAXD and WAXD studies were performed at 32 °C, using a multi-purpose Peltier gel-holder stage on a Xeuss 3.0 instrument (Xenocs, France), with an X-ray beam generated by a CuK_α radiation source (λ = 1.542 Å). Before measurements, samples were stored in a desiccator containing saturated K_2SO_4 solution at 97% relative humidity. The samples, of both PPy-SC and SC, were sandwiched in a gel holder and sealed between two Kapton films (DuPontTM Kapton®, 0.013 mm thickness, Goodfellow, England) using an O-ring spacer. A Pilatus3 R 300 K hybrid photon counting detector with a sample-to-detector distance (STDD) of 800 mm (SAXD) and 285 mm (WAXD) was used. The samples were exposed for 3 h for SAXD and 1 h for WAXD. The two STDDs covered the q-range $0.01 \leq q\ (nm^{-1}) \leq 18$, where q is the scattering vector defined as $|\boldsymbol{q}| = q = 4\pi/\lambda \sin(\theta/2)$ and θ is the scattering angle. Azimuthal integration of the 2D patterns provided the 1D diffraction curves, which were corrected for background scattering and normalized to the direct beam, using the Xenocs XSACT software (version 2.6). Silver behenate was used to calibrate the q-scale. Background subtraction of two empty Kapton films was performed. The intensity data of SAXD and WAXD measurements were normalized (Eq. (1)) for a selected range of q values.

$$I_{normalized} = \frac{I_{measured} - I_{minimal}}{I_{maximal} - I_{minimal}} \cdot 100\% \quad (1)$$

Where $I_{normalized}$ – normalized value (%) of X-ray scattering intensity, $I_{measured}$ – a measured value of X-ray scattering intensity, $I_{minimal}$ and $I_{maximal}$ – the smallest and the largest values of X-ray scattering intensity for a selected range of q.

2.8. Dynamic Vapor Sorption (DVS)

Water sorption-desorption isotherms of SC, PPy-SC and PPy flakes were recorded at 25 °C using a DVS microbalance (Q5000 SA, TA Instruments - Waters Sverige AB, Sollentuna, Sweden). Before measurements, samples were dried in desiccator. Dried SC sheets, PPy-SC sheets, or PPy flakes, weighing 3 mg, were placed in a glass beaker, loaded onto the DVS microbalance, and sealed in the sample chamber to allow control of the relative humidity (RH). The sample was first exposed to dry N_2 gas (*i.e.*, 0% RH) at 35 °C until a stable reading was obtained. Next, the temperature was changed to 25 °C (0% RH) until a stable dry weight reading was obtained. The RH was then ramped up from 0 to 98% RH in increments of 2%. The mass of the sample was continuously measured by the DVS microbalance to allow the calculation of water sorption isotherms; the water content is given in weight percentage (W_t%) and calculated by $(m_{tot}\text{-}m_{dry})/m_{tot}$, where m_{tot} is the total mass of the sample including water at a given time and m_{dry} is the dry mass of the sample at 0% RH and 25 °C.

3. Results and discussion

3.1. Polypyrrole deposition on porcine skin membranes: microscopy and EIS

In this work, polymerization of pyrrole producing a conducting polypyrrole (PPy) on the surface of porcine skin was studied *in vitro*. The polymerization was carried out in a Franz cell setup (Fig. 1A). The

pyrrole solution (0.15M) was placed in the lower Franz cell compartment with the dermal side of the skin exposed to the solution. The oxidant, $FeCl_3$ solution (0.06 M), was charged into the upper compartment of the Franz cell with the SC side of the skin exposed to the solution. The polymerization process was easily followed by digital USB microscope (× 1000, China), proving that PPy deposits on the top of the SC. Already, after 18 h of polymerization, the skin membrane appeared completely black (Fig. 1B).

Upon removal of the SC using trypsin solution in PBS (0.2%), the underlying tissue revealed its natural color (Fig. 1C), indicating that the PPy network is primarily connected to the outermost side of the SC. This observation is further supported by FTIR spectra, which showed PPy absorbance peaks only on the outermost, $FeCl_3$ exposed, side of SC (Fig. S1).

Altogether, these results prove that pyrrole monomers, present on the dermal side of the skin in the Franz cell, effectively permeated the skin membrane, including the SC, met the low-permeable Fe^{3+} ions, and polymerized to PPy right on the top of the SC (Fig. 1A). This interfacial polymerization resulted in a continuous coating rather than dispersed particles. A similar phenomenon has been observed in other membrane systems [24]. A likely explanation is that nucleation sites at the interface adhere to the surface, promoting continuous polymer growth instead of free particle formation. To the best of our knowledge, this is the first disclosure of a Franz cell-based methodology enabling seamless deposition and studies of conducting polymer on skin membranes *in vitro*. The approach shown in Fig. 1A was also confirmed to be successful with the alternative monomer aniline, which formed a deposited polyaniline layer, demonstrating that the method is applicable in a more general manner (see Fig. S2). Theoretically, the Franz cell-based approach could also be applied to oxidative 3,4-ethylenedioxythiophene (EDOT) polymerization, as PEDOT has recently attracted significant interest in the bioelectronic field [25–28].

Overall, the Franz cell-based setup is suitable for depositing polymers whose monomers penetrate the SC and participate in oxidative polymerization on the SC side of the skin. This *in vitro* approach is especially useful for studying conducting polymer/skin interfaces before biocompatible recipes are available for creating bioelectronic skins.

To assess the PPy-SC interface, the PPy-modified skin membranes were extensively studied by EIS. Impedance data of three replicate skin membranes, denoted as n = 1, n = 2, and n = 3, before and after PPy deposition are presented as Nyquist plots in Fig. 2. The shape of the Nyquist plots, corresponding to both unmodified (Fig. 2, filled circles) and PPy-modified skin membranes (Fig. 2, empty circles), clearly reveal a single depressed semicircle. The semicircle shape in Nyquist plots is commonly observed for skin membranes and reflects a combination of transdermal (resistive) and charging (capacitive) currents flowing in parallel [13,29]. The general features of the Nyquist plots are similar across all replicate skin membranes investigated, with a noticeable decrease in the diameter of the semicircle after PPy deposition. Some changes are also observed in the data patterns outside the semicircles (data at low frequencies, points on the right-hand side of the curves, Fig. 2). However, these changes are inconsistent. Thus, only high-frequency EIS data were modelled by the equivalent circuit shown in Fig. 2D, *i.e.*, the circuit that captures the main impedance characteristics of skin in electrolyte solutions.

The resistance of the electrolyte solution is represented by the resistor (R_s). The R_s is connected to a parallel circuit comprised of a resistor (R_m) and a constant phase element (CPE) representing the resistance and capacitance properties of skin membrane, respectively. The CPE accounts for the non-ideal capacitance of the skin membrane. CPE module value is usually regarded as an effective capacitance (C_{eff}) for easy relating to the dielectric constants and geometric dimensions of

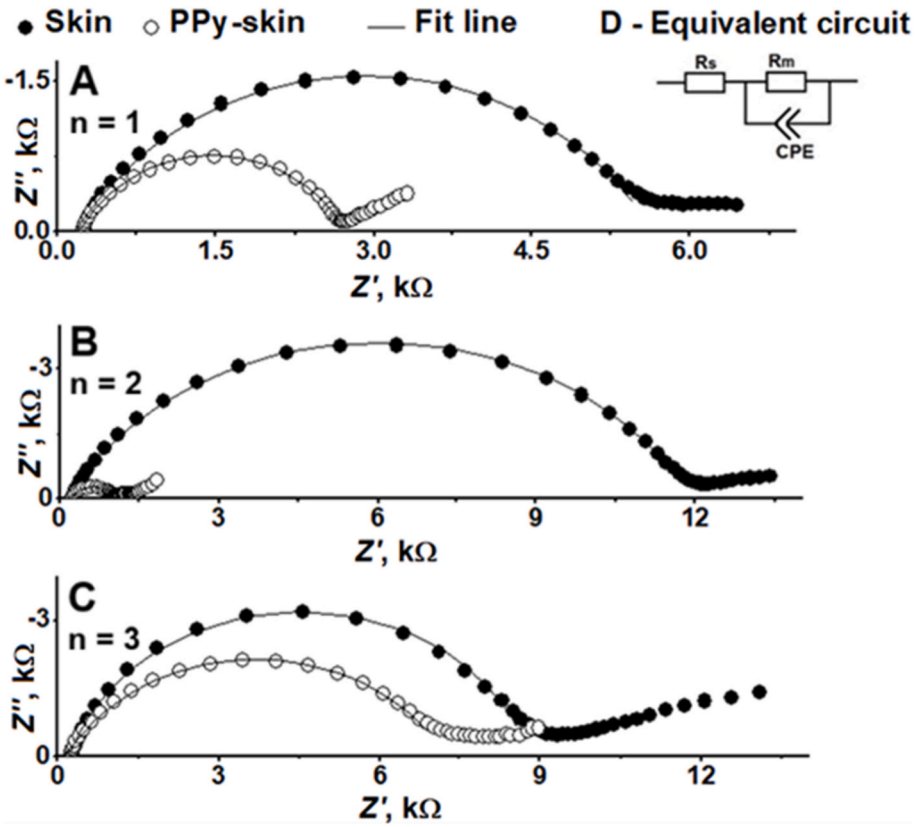

Fig. 2. Representative EIS data were obtained before and after the modification of skin membranes with polypyrrole; data were obtained from three replicate skin membranes (n = 1, n = 2, n = 3). The equivalent circuit used to fit and analyze the EIS data is shown in (**D**) where R_s is solution resistance, R_m is membrane resistance, and CPE represents a constant phase element used to estimate the effective capacitance (C_{eff}) of the skin membranes.

skin membranes [30,31]. Considering a low permeability of ions through SC *vs* dermal layer of the skin, the values of R_m and C_{eff} primarily reflect the barrier properties of SC. In simple terms, R_m represents the resistance to transdermal (through SC) transport of ions [22,23]. C_{eff} reflects double-layer charging of ion-impermeable interfaces made of SC lipids, lipid matrix, and lipid-protein domains. The dielectric properties/constants these biomaterials strongly influence C_{eff}, Eq. (2) [13,29,32–34].

$$C_{eff} = \varepsilon_0 \varepsilon_r \frac{A}{d} \tag{2}$$

where C_{eff} (F) is effective capacitance, ε_0 - the permittivity of free space (8.854×10^{-12} F·m^{-1}), ε_r is a relative dielectric permittivity of the medium (biomaterials) separating the charges, A (m^2) and d (m) are the surface area and the thickness of the capacitive domains in the *SC*, respectively.

The impedance parameters of three replicate skin membranes, obtained by fitting the EIS data to the equivalent circuit (Fig. 2D), are presented in Fig. 3 and Table S1. The R_m and C_{eff} values vary considerably for each replicate skin membrane. This variability is typical for skin due to biological differences in molecular composition of the SC, the number of hair follicles and sweat glands [31,35,36]. Despite this variability, the changes in impedance properties of the skin after PPy modification are well-defined. Firstly, PPy modification causes a decrease in R_m. Secondly, an increase in C_{eff} is observed for all skin membranes (Fig. 3). These changes should be due to the deposition of conducting PPy on the skin membranes since the same changes were reproduced in control experiments done with cellulose membranes (Fig. S3 and Table S2).

Notably, the general shape of the high-frequency semicircle (Fig. 2) remained similar before and after PPy modification, despite changes in radius, with the CPE n value showing no systematic variation (Table S1). This indicates that no additional EIS feature (e.g., PPy charging/discharging) emerged in this range, such that the spectrum remains dominated by the SC's barrier to ion transport – the most resistive process. Additionally, the conductive properties of PPy on skin were confirmed by a 100-fold reduction in surface resistance of PPy-coated membranes (see Supplementary Information).

The decrease in R_m and the increase in C_{eff} observed after modifying skin with PPy might be related not only to the formation of PPy on the SC, but also to prolonged exposure to aqueous solutions [37–39]. Therefore, control experiments were performed by exposing skin membranes in Franz cells for 24 h to: (i) pyrrole solution (0.15 M) on both sides of the skin (Fig. S4A), (ii) deionized water on both sides of the skin (Fig. S4B), and (iii) $FeCl_3$ (0.06 M) solution on the SC side and deionized water on the dermal side of the skin (Fig. S4C). All three control studies (i, ii, and iii) resulted in increased R_m and increased C_{eff} (Fig. S5). These control experiments confirm that the observed decrease in R_m (Fig. 3A) is related to the PPy modification and not to prolonged exposure of the skin membrane to aqueous solutions. However, the increase in C_{eff} after PPy modification (Fig. 3B) can be attributed to both the formation of the PPy network and the hydration of the SC, contributing to an increased dielectric constant of the PPy-SC membranes, Eq. (2).

3.2. *Impedance characteristics of porcine skin in solutions with varying KCl concentrations: Evidence of apparent nanopores in skin*

To understand the structural details of the PPy/skin interface, we addressed the hypothesis that the observed changes in the impedance properties of skin membranes after PPy deposition might arise from PPy occupying nanoscopic defects in the SC lipid matrix, which can form dynamically through grain-boundary separations and lattice vacancies that generate multimolecular voids.

According to the four permeation pathways model [21], the diffusion of small hydrophilic molecules and ions, in our case Fe^{3+}, can occur through nanosized defects in the SC lipid matrix [40]. Thus, it is plausible that pyrrole molecules permeate lipid lamellae structures of SC and encounter the ferric ions in SC nanopores, causing immediate PPy deposition in the nanopores. This would result in reduced R_m and increased C_{eff}. Alternatively, pyrrole monomers, due to their small size and relative lipophilicity, can diffuse into the lipid lamellae of the SC. Upon reaching regions containing Fe^{3+}, in situ oxidative polymerization may occur. Such localized polymer growth at the SC/Fe^{3+} interface could disrupt lipid packing and generate structural defects (e.g., cracks or pore-like discontinuities) that enhance ionic permeability and may propagate toward deeper SC layers.

Even though pore size in SC has been related to membrane resistance in past research [41], to the best of our knowledge, the behavior of skin nanopores in electrolytes of different concentrations has not been studied using EIS to date. Nevertheless, this approach is well-established for analyzing electrolyte-filled nanopores in silica [42]. Essentially, the method involves resistance measurement of nanopore-containing membranes at different electrolyte concentrations. At high electrolyte concentrations, C, the R_m follows a $1/C$ dependence as described by general R *vs* $1/C$ Eq. (3) and illustrated in Fig. 4.

$$R = \rho \cdot \frac{l}{A} = \frac{1}{F \sum_i z_i u_i c_i} \cdot \frac{l}{A} \tag{3}$$

R is a resistance (Ω), ρ – resistivity of the solution (Ω m), z_i – charge of an

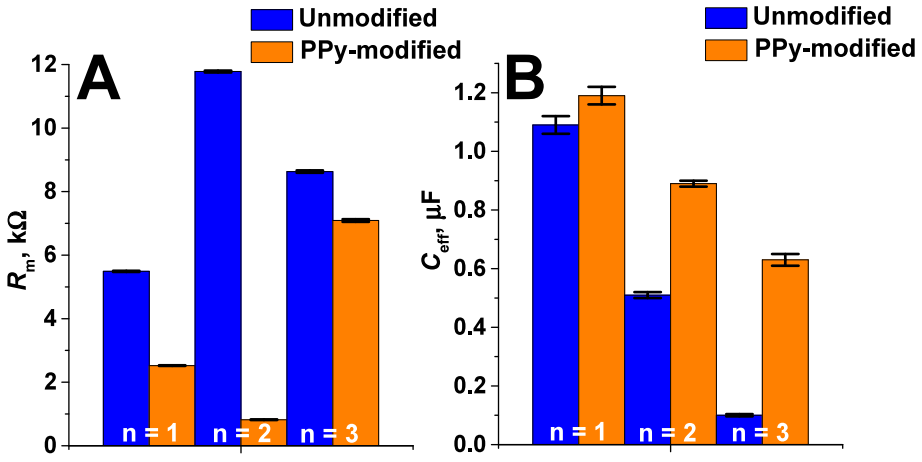

Fig. 3. Values of **(A)** R_m and **(B)** C_{eff} obtained for skin before and after PPy deposition; C_{eff} is assumed to be equal to Q value of CPE. Three replicate skin membranes are denoted as n = 1, n = 2, and n = 3. Errors represent the uncertainty of the R_m and C_{eff} values obtained during the fit of impedance data shown in Fig. 2.

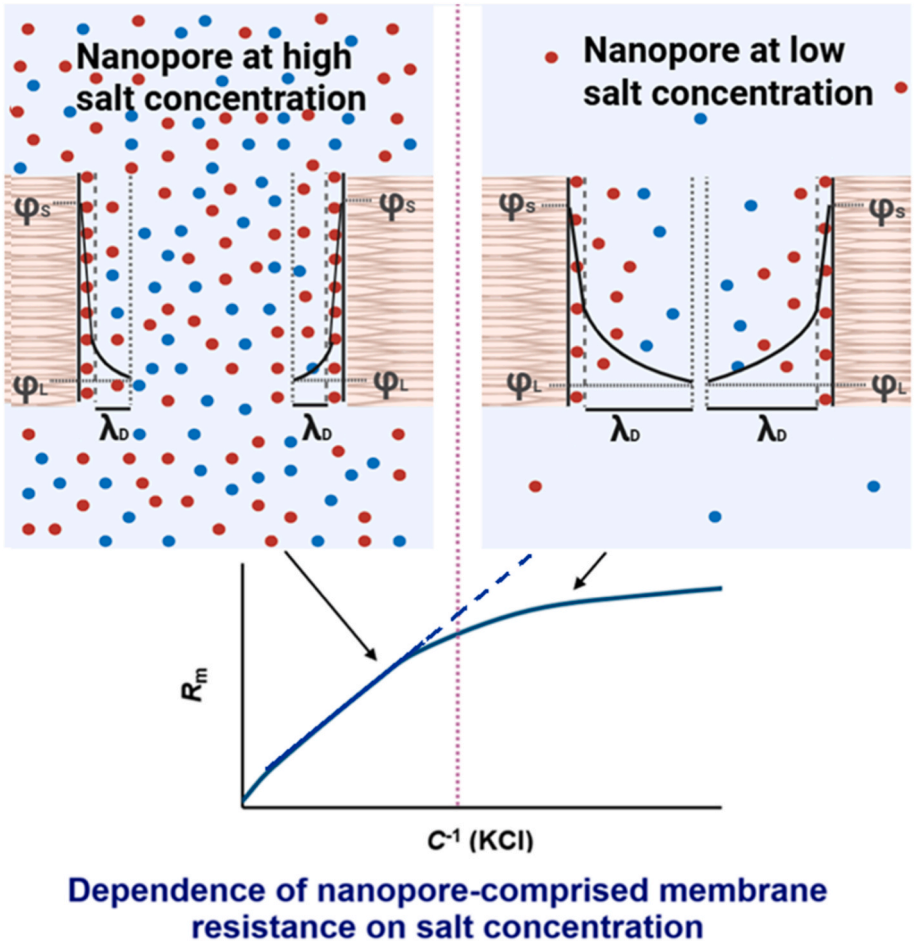

Fig. 4. Schematic representation of EDL dimensions (λ_D) at nanopore walls and electrolyte ion concentration in nanopores *vs* bulk electrolyte. φ_S and φ_L represents the potential at the surface of solid phase (skin) and in the liquid phase (KCl solution), respectively. λ_D - Debye length (thickness of the diffuse layer of EDL). At high salt concentration (small λ_D), the conductivity of the solution in a nanopore is similar to the conductivity of the solution outside the nanopore (we can call this a volume conductivity). However, with the decrease of the electrolyte concentration, the Debye length at the nanopore inner wall/solution interface increases and leads to overlapping EDL. At this condition, the conductivity inside the nanopore is higher than that of the surrounding diluted electrolyte. The conductivity is dominated by surface-confined ions. Created with BioRender.com (publication license granted to Sebastian Björklund/Malmö University).

ion, F – Faraday's constant (96 485.3 C mol^{-1}), u_i – mobility of an ion (7.62×10^{-8} m^2 s^{-1} V^{-1} for K^+ and 7.91×10^{-8} m^2 s^{-1} V^{-1} for Cl^-), c_i – concentration of the ions (K^+ and Cl^-, in case of electrolyte made only of KCl solution). l is the path length for the ion flow, which is equal to the distance between the potential measuring electrode probes (~2.5 cm) for the case of assessing solution resistance (no membrane), or l is the thickness of the *SC* layer (~10 μm) in the case of assessing membrane resistance. A – cross-sectional area (0.64 cm^2) of the Franz cell, which defines the skin membrane area in contact with the electrolyte solution.

The effect of nanopores on EIS parameters of skin can be assessed by diluting the electrolyte in a Franz cell. This leads to an extension of the electrical double layers (EDL) at the nanopores in SC, eventually causing EDL overlap (Fig. 4). At the overlap, due to the need for screening of the charges on nanopore walls, the electrolyte concentration within the nanopore cannot be easily reduced by further electrolyte dilution. This results in a much weaker R_m dependence on $1/C$, as illustrated in Fig. 4. The electrolyte concentration, at which the linearity the R_m *vs* $1/C$ no longer holds, can be used to estimate the EDL dimension (Debye length) at the EDL overlap, Eq. (4). Consequently, and simplistically, the nanopore dimensions could be estimated as two times the Debye length.

$$\lambda_D = \sqrt{\frac{\varepsilon_0 \varepsilon_r RT}{2F^2 C}} \quad (4)$$

In Eq. (4), λ_D is the Debye length (m) and C is the concentration of KCl in solution (mol m^{-3}), while all other parameters follow Eqs. (2) and (3). Eq. (4) can be applied to calculate λ_D for a symmetric monovalent electrolyte.

To test the hypothesis that PPy might deposit in SC nanopores and to explore the EIS approach for assessing nanopore presence in skin membranes, we conducted EIS measurements on unmodified and PPy-modified skin membranes in KCl solutions of different concentrations, ranging from 0.2 M to 0.01 M. Raw impedance data (Figs. S6 and S7) were fitted to the equivalent circuit (Fig. 2D), yielding R_m dependencies on the KCl concentration, Fig. 5.

The values of R_m, even at the highest KCl concentrations (Fig. 5), showed no linear relation to the reciprocal of the KCl concentration, which confirms a considerable role of EDL in nanopores in determining R_m. Meanwhile, the values of R_s across the entire experimental concentration range (Fig. S8) were linearly related to $1/C$ of the KCl concentration as expected for resistance defined by bulk conductivity. The individual values for the three investigated replicate membranes (n = 1, n = 2 and n = 3) are listed in Tables S3–S5. In supplementary information we attempted modelling of R_m *vs* $1/C$ for one of membrane giving a satisfactory result assuming that the membrane contains 1.2×10^8 nanopores with a radius of 1 nm and 1×10^7 nanopores with a radius of 6 nm (Fig. S9). These dimensions are bigger than diameters of 0.5-1.6 nm SC nanopores that were estimated previously [43,44]. It is very likely that due to assumptions of surface potentials, lengths, and

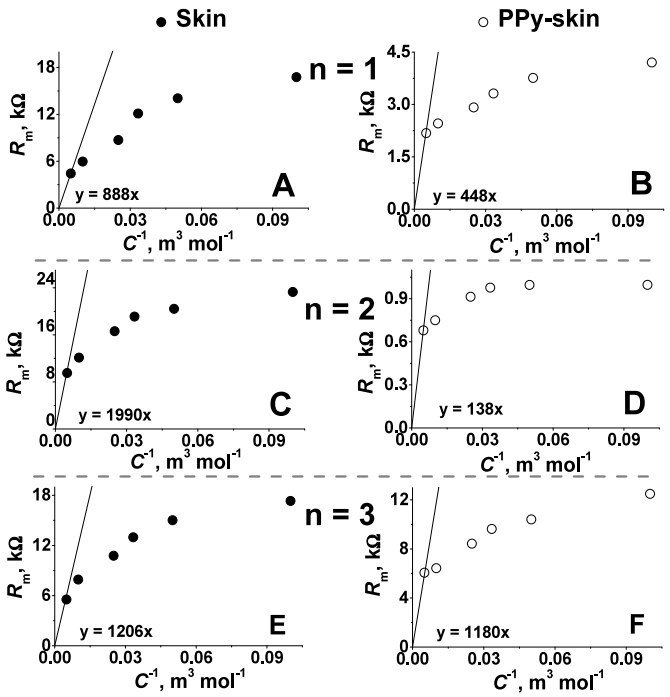

Fig. 5. Dependence of skin membrane resistance on C^{-1} (concentration of KCl). The R_m was determined by EIS measurements of skin membranes placed in Franz cells, in contact with equimolar KCl solutions on both sides of the skin. **A**, **C** and **E** – R_m of unmodified porcine skin membranes (n = 1, n = 2, and n = 3 are three replicate skin membranes). **B**, **D** and **F** - R_m of corresponding skin membranes after modification with PPy.

density of the nanopores in SC (see SI) we overestimate the diameter by 2-3 times. It is not excluded that freezing of skin membranes for their storage increases dimensions of nanopores and number of nano defects.

The data in Fig. 5 show that the PPy-modified skin has similarly shaped R_m *vs* $1/C$ dependency as unmodified skin membranes. This might suggest that PPy modification has no considerable effect on the size of the nanopores or nano defects in the SC. However, the R_m values are significantly lower, being approximately 6 ± 5 kΩ for PPy-modified skin *vs* 18 ± 3 kΩ for unmodified skin. It is possible that PPy modification enhances charge transfer through nanopores/defects, *e.g. via* charge carriers along the polymer backbone, leading to increased skin conductivity (e.g., as modelled in SI assuming higher value of nanopore surface potential). Alternatively, PPy modification might increase the number of nanopores. Both factors (increased number of nanopores and pore conductivity) are expected to contribute to increased skin conductivity. It is important to note that both effects indicate that nanopore and nano defect structures in SC are involved in building skin/PPy interfaces.

3.3. DVS and X-ray diffraction analysis of PPy modified stratum corneum

To gain deeper insight into the mechanism by which pyrrole polymerizes within the SC composite membrane, we conducted complementary Dynamic Vapor Sorption (DVS) and Small-Wide Angle X-ray Diffraction experiments. These techniques probe functional and structural aspects of both the lipid matrix and the keratin filaments of the SC. Pyrrole is a low-molecular-weight, hydrophobic molecule ($K_o/_p = 5.6$ [45]) and is therefore expected to permeate the SC predominantly through the lipid lamellar regions via free-volume diffusion, a well-established pathway for small organic molecules with molecular radii <0.4 nm and $K_o/_p > 1$ [21,37]. This transport mechanism predicts a relatively homogeneous penetration of pyrrole through the lipid matrix. Consequently, if pyrrole were to polymerize primarily within the lipid lamellae, substantial alterations in the molecular organization of the SC lipid matrix would be anticipated. Conversely, if polymerization predominantly involved the keratinous corneocytes, changes in the characteristic diffraction peak associated with soft keratin would be expected.

The water sorption–desorption isotherms obtained from DVS measurements of intact SC and PPy-modified SC sheets (PPy-SC) show that PPy modification has only a minor effect on the SC hydration process (Fig. 6). Specifically, the PPy modification results in a slight reduction in water sorption. However, the overall shape of the water content versus relative humidity curve is similar for both intact SC (Fig. 6A) and PPy-modified SC (Fig. 6B), exhibiting a steep increase in water content at relative humidities above approx. 60% which is typical for porcine (and human) SC [33]. Meanwhile, in case of DVS measurement of PPy flakes (Fig. 6C), it is obvious that PPy retains much less water than SC (Fig. 6A). The low water uptake by pure PPy flakes (Fig. 6C) indicates rather weak interactions between PPy and water, being consistent with the fact that chloride-doped PPy exhibits a contact angle with water between 80° and 90° [34], making it neither strongly hydrophilic nor strongly hydrophobic.

It is also worth noting that the keratin-rich corneocytes in SC (of human or pig) have been associated with the formation of water pools in the intercellular regions, and are considered to be the main component determining the water content in SC at different relative humidities [35–38]. Therefore, the comparison of water sorption isotherms of porcine SC *vs* PPy modified SC is expected to reflect substantial change of water retention ability of keratin structures due to their PPy modification. Considering that the overall water sorption characteristics of the SC within the PPy-modified SC remain largely unaffected by the PPy modification, it can be concluded that PPy does not disturb the keratin structures in SC. The slight decrease in water content observed in PPy-modified SC (Fig. 6B) compared with intact SC (Fig. 6A) can be attributed to the lower relative mass of SC in the PPy-SC sheets due to the presence of PPy, rather than direct interaction or disruption of keratin structures.

To investigate the effect of PPy modification on the molecular structure of SC, both unmodified and PPy-modified SC samples were analyzed using small and wide-angle X-ray diffraction (SAXD and WAXD). The results are presented in Fig. 7A and B, respectively. Briefly, the SAXD data show broad shoulders around q-values of 0.5 nm^{-1} and 1 nm^{-1}, as well as a weaker diffraction shoulder at 1.5 nm^{-1}. This is consistent with previous diffraction studies on porcine SC [13,46,47], suggesting that the SC lipid matrix is organized into at least one lamellar phase with repeat distances of 13 nm. The WAXD data in Fig. 7B show a clear peak around q = 15.2 nm^{-1} (0.41 nm in d-spacing), corresponding to a hexagonal lateral packing of the SC lipid acyl chains [13,47]. The broad diffraction peak with a maximum around q = 6 nm^{-1} (0.95 nm in d-spacing) is attributed to the distance between adjacent protein chains (interatomic vectors), providing an estimate of the interchain separation of protein monomers in soft keratin filaments [48,49].

A closer analysis of the normalized intensity indicates that PPy modification of SC sheets results in a slight decrease in the scattering intensity from the lipid lamellar structures in the SAXD regions (Fig. 7C) and of the diffraction peak corresponding to lipids with a hexagonal lateral unit cell (Fig. 7E). This suggests that the polymerization process causes minor disordering of the SC lipids. The normalized intensity of the broad diffraction peak from soft keratin remained unaffected (Fig. 7D), indicating that PPy modification does not influence the keratin structures of the corneocytes. These findings are in line with the DVS data (Fig. 6), showing that the overall water sorption characteristics of the SC sheets remain largely unaffected by the PPy modification (i.e., the sorption-desorption characteristics are dominated by the keratin). Therefore, the X-ray diffraction data indicate that the PPy modification primarily affects the structure of the lipid layer of the SC, rather than the keratin.

Although the X-ray data are based on a single sample per condition

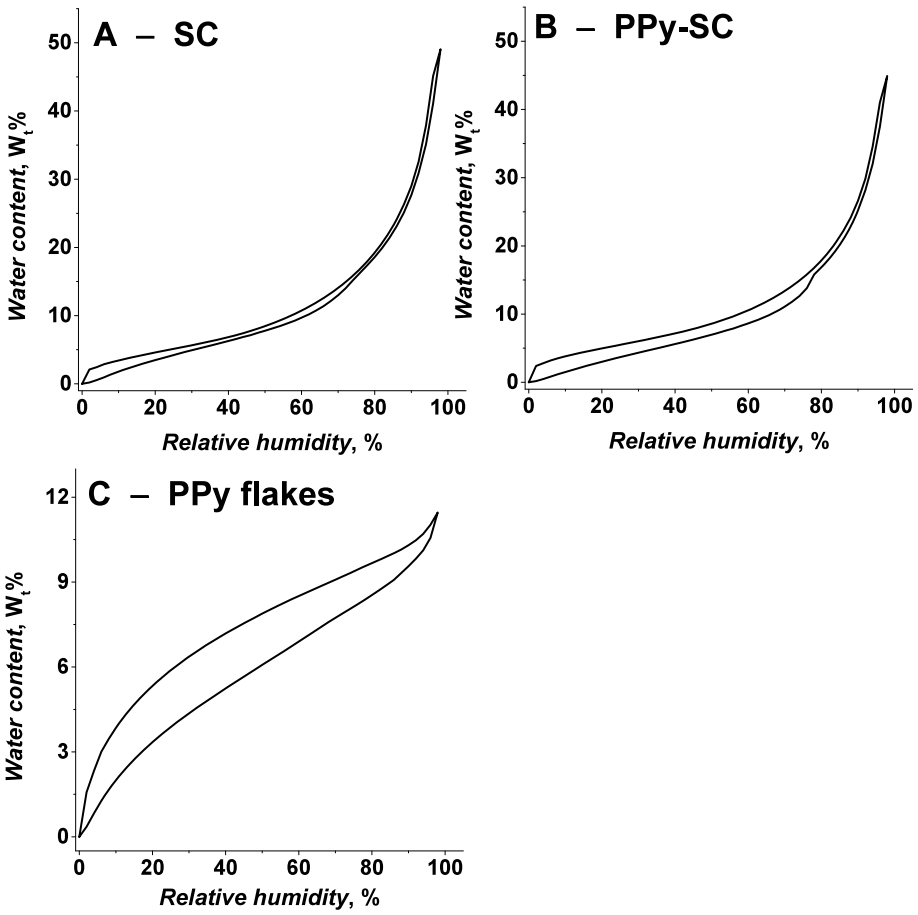

Fig. 6. Relationship between sample water content and relative humidity for different samples: unmodified SC (**A**), PPy-modified SC (**B**), and PPy flakes (**C**).

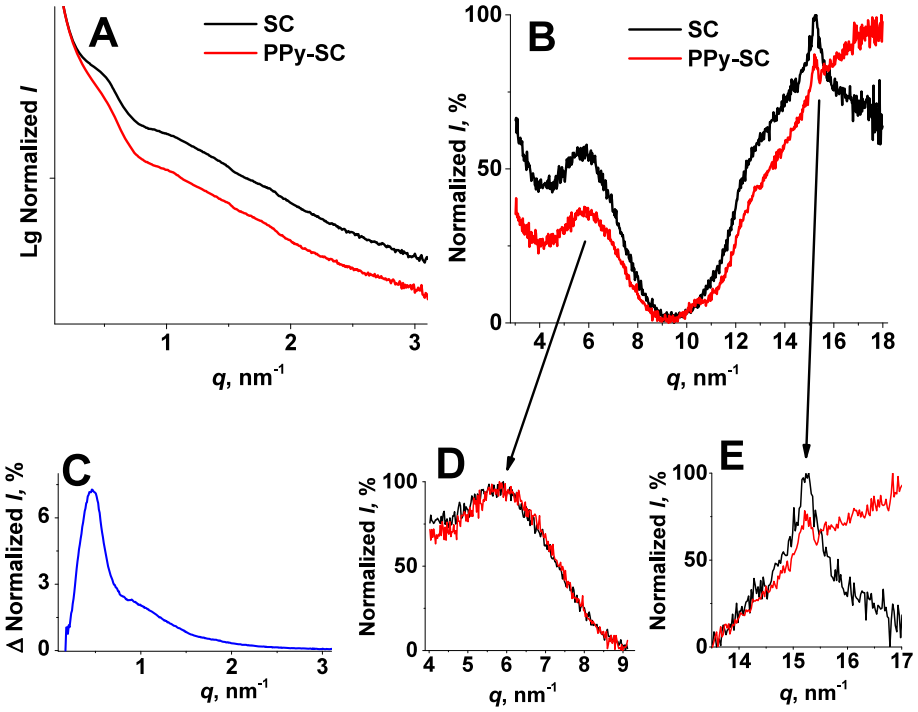

Fig. 7. SAXD (**A**) and WAXD (**B**) spectra of unmodified and PPy-modified *SC*. Values of logarithmic intensity (Lg *I*) in SAXD data were normalized in the *q* range from 0.1 nm^{-1} to 3.5 nm^{-1}, while values of intensity (*I*) in WAXD data were normalized in the *q* range from 3.0 nm^{-1} to 18.0 nm^{-1}. **C** - Difference between normalized *I* values (Δ Normalized *I*, %) calculated by subtracting normalized *I* values obtained during the PPy-SC investigation from normalized *I* values obtained during the *SC* investigation. **D** and **E** - *I* values (WAXD data) normalized in q ranges from 4.0 nm^{-1} to 9.1 nm^{-1} and from 13.5 nm^{-1} to 17.0 nm^{-1}, respectively.

and should therefore be interpreted with caution, the observations align with the EIS results. Together, the experimental data suggest that PPy is present not only on the SC surface but also forms a continuous conducting junction across the SC, which may account for the weakened diffraction peaks associated with the lipid matrix – the only continuous structural phase of the SC composite membrane. Optical microscopy of cross-sections of PPy-modified porcine skin (Fig. S10) confirms that PPy covers the SC, with occasional aggregates observed in the dermal region. Tape-stripping experiments (Fig. S11) further show that detectable PPy remains on the skin even after 40 consecutive strips, indicating strong adhesion to the SC and deposition within appendages and furrows that protect the polymer from mechanical removal. However, these images provide no evidence for homogeneous polymerization within the skin layers. Thus, the reduction in SC resistance following PPy formation is likely explained by the development of microscopic conductive pathways within the SC – potentially following the lipid matrix – that together form a coherent conductive junction across the barrier.

4. Conclusions

This study presents a novel approach to modify porcine skin membranes with the conducting polymer polypyrrole, significantly altering membrane electrical properties. For the first time, direct pyrrole polymerization on skin membranes has been demonstrated using a Franz cell-based methodology. The evolving bioelectronic structure is characterized by seamless conducting polymers/skin interphase. Strongly diminished PPy-skin membrane resistance and increased effective capacitance suggest that PPy forms a conductive network across the stratum corneum, enhancing transdermal charge transfer and improving the ion storage capabilities of PPy-skin membranes.

For the first time, electrochemical impedance measurements are used to study the manifestation of skin nanopores in electrolytes of different concentrations. Our findings indicate that PPy modification likely increases the number of nanopores/defects within the SC. This study uniquely integrates EIS, dynamic vapor sorption, and SAXD/WAXD to demonstrate that PPy influences the molecular lipid organization in the SC, mainly affecting structures which are in close contact with the electrolyte solution at the skin/electrolyte interface.

The innovative methodology and insights from this study present a novel *in vitro* approach for advancing future research on organic electronics-skin interactions. We emphasize that developing and refining new *in vitro* methods is important to minimize the reliance on *in vivo* studies that may lack sufficient *in vitro* validation. The approach also enables studies of bioelectronic systems on skin made of toxic components thus providing data and methodology which should be helpful in searching for biocompatible solutions. The described methodology is expected to facilitate the study and optimization of seamless interfaces between electronics and skin, focusing on key aspects such as adhesion, stability, and biocompatibility of conducting polymers on skin.

CRediT authorship contribution statement

Povilas Virbickas: Writing – review & editing, Writing – original draft, Visualization, Investigation, Formal analysis, Data curation, Conceptualization. **Sebastian Björklund:** Writing – review & editing, Writing – original draft, Supervision, Methodology, Formal analysis, Conceptualization. **Skaidre Jankovskaja:** Investigation, Formal analysis, Data curation. **Emelie Nilsson:** Investigation, Formal analysis, Data curation. **Aušra Valiūnienė:** Writing – review & editing, Writing – original draft, Methodology. **Johan Engblom:** Writing – review & editing, Writing – original draft, Conceptualization. **Tautgirdas Ruzgas:** Writing – review & editing, Writing – original draft, Supervision, Methodology, Formal analysis, Conceptualization.

Declaration of competing interest

The authors declare that they have no known competing financial interests or personal relationships that could have appeared to influence the work reported in this paper.

Acknowledgements

We acknowledge the Knowledge Foundation (20190010, profile Biobarriers). TR and JE thank the Gustaf Th. Ohlsson Foundation.

Appendix A. Supplementary data

Supplementary data to this article can be found online at https://doi.org/10.1016/j.mtadv.2026.100773.

Data availability

Data will be made available on request.

References

[1] L. Lipani, B.G.R. Dupont, F. Doungmene, F. Marken, R.M. Tyrrell, R.H. Guy, et al., Non-invasive, transdermal, path-selective and specific glucose monitoring via a graphene-based platform, Nat. Nanotechnol. 13 (2018) 504–511, https://doi.org/10.1038/s41565-018-0112-4.
[2] C. Zhao, J. Park, S.E. Root, Z. Bao, Skin-inspired soft bioelectronic materials, devices and systems, Nat. Rev. Bioeng. 2 (2024) 671–690, https://doi.org/10.1038/s44222-024-00194-1.
[3] A.M. Vargason, A.C. Anselmo, S. Mitragotri, The evolution of commercial drug delivery technologies, Nat. Biomed. Eng. 5 (2021) 951–967, https://doi.org/10.1038/s41551-021-00698-w.
[4] M.R. Prausnitz, R. Langer, Transdermal drug delivery, Nat. Biotechnol. 26 (2008) 1261–1268, https://doi.org/10.1038/nbt.1504.
[5] M. Morin, S. Björklund, S. Jankovskaja, K. Moore, M.B. Delgado-Charro, T. Ruzgas, et al., Reverse iontophoretic extraction of skin cancer-related biomarkers, Pharmaceutics 14 (2021), https://doi.org/10.3390/pharmaceutics14010079.
[6] R. Parhi, P. Suresh, S. Patnaik, Physical means of stratum corneum barrier manipulation to enhance transdermal drug delivery, Curr. Drug Deliv. 12 (2015) 122–138, https://doi.org/10.2174/1567201811666140515145329.
[7] R. Balint, N.J. Cassidy, S.H. Cartmell, Conductive polymers: towards a smart biomaterial for tissue engineering, Acta Biomater. 10 (2014) 2341–2353, https://doi.org/10.1016/j.actbio.2014.02.015.
[8] S. Inal, J. Rivnay, A.-O. Suiu, G.G. Malliaras, I. McCulloch, Conjugated polymers in bioelectronics, Acc. Chem. Res. 51 (2018) 1368–1376, https://doi.org/10.1021/acs.accounts.7b00624.
[9] V.C. Hoang, A. Shafaat, S. Jankovskaja, V.G. Gomes, T. Ruzgas, Franz cells for facile biosensor evaluation: a case of HRP/SWCNT-based hydrogen peroxide detection via amperometric and wireless modes, Biosens. Bioelectron. 191 (2021) 113420, https://doi.org/10.1016/j.bios.2021.113420.
[10] Medicine USNLo, Hazardous substances data bank [Available from: https://pubchem.ncbi.nlm.nih.gov/source/HSdb.
[11] J. Stejskal, M. Trchová, P. Bober, Z. Morávková, D. Kopecký, M. Vrňata, et al., Polypyrrole salts and bases: superior conductivity of nanotubes and their stability towards the loss of conductivity by deprotonation, RSC Adv. 6 (2016) 88382–88391, https://doi.org/10.1039/C6RA19461C.
[12] M. Omastová, M. Trchová, J. Kovářová, J. Stejskal, Synthesis and structural study of polypyrroles prepared in the presence of surfactants, Synth. Met. 138 (2003) 447–455, https://doi.org/10.1016/S0379-6779(02)00498-8.
[13] S. Björklund, T. Ruzgas, A. Nowacka, I. Dahi, D. Topgaard, E. Sparr, et al., Skin membrane electrical impedance properties under the influence of a varying water gradient, Biophys. J. 104 (2013) 2639–2650, https://doi.org/10.1016/j.bpj.2013.05.008.
[14] N. Labecka, M. Szczepanczyk, E. Mojumdar, E. Sparr, S. Björklund, Unraveling UVB effects: catalase activity and molecular alterations in the stratum corneum, J. Colloid Interface Sci. 666 (2024) 176–188, https://doi.org/10.1016/j.jcis.2024.03.200.
[15] M.F. Planche, J.C. Thiéblemont, N. Mazars, G. Bidan, Kinetic study of pyrrole polymerization with iron (III) chloride in water, J. Appl. Polym. Sci. 52 (1994) 1867–1877, https://doi.org/10.1002/app.1994.070521304.
[16] D.D. Ateh, P. Vadgama, H.A. Navsaria, Culture of human keratinocytes on polypyrrole-based conducting polymers, Tissue Eng. 12 (2006) 645–655, https://doi.org/10.1089/ten.2006.12.645.
[17] S. Cui, J. Mao, M. Rouabhia, S. Elkoun, Z. Zhang, A biocompatible polypyrrole membrane for biomedical applications, RSC Adv. 11 (2021) 16996–17006, https://doi.org/10.1039/D1RA01338F.
[18] P. Humpolíček, V. Kašpárková, J. Pacherník, J. Stejskal, P. Bober, Z. Capáková, et al., The biocompatibility of polyaniline and polypyrrole: a comparative study of

their cytotoxicity, embryotoxicity and impurity profile, Mater. Sci. Eng. C 91 (2018) 303–310, https://doi.org/10.1016/j.msec.2018.05.037.
[19] K. Zhang, M. Chen, G.K.E. Scriba, M.H. Abraham, A. Fahr, X. Liu, Human skin permeation of neutral species and ionic species: extended linear free energy relationship analyses, J. Pharmaceut. Sci. 101 (2012) 2034–2044, https://doi.org/10.1002/jps.23086.
[20] M. Tarnowska, S. Briançon, J. Resende de Azevedo, Y. Chevalier, M.-A. Bolzinger, Inorganic ions in the skin: allies or enemies? Int. J. Pharm. 591 (2020) 119991 https://doi.org/10.1016/j.ijpharm.2020.119991.
[21] S. Mitragotri, Modeling skin permeability to hydrophilic and hydrophobic solutes based on four permeation pathways, J. Contr. Release 86 (2003) 69–92, https://doi.org/10.1016/S0168-3659(02)00321-8.
[22] H.E. Boddé, I. van den Brink, H.K. Koerten, F.H.N. de Haan, Visualization of in vitro percutaneous penetration of mercuric chloride; transport through intercellular space versus cellular uptake through desmosomes, J. Contr. Release 15 (1991) 227–236, https://doi.org/10.1016/0168-3659(91)90114-S.
[23] R.O. Potts, R.H. Guy, M.L. Francoeur, Routes of ionic permeability through mammalian skin, Solid State Ionics 53–56 (1992) 165–169, https://doi.org/10.1016/0167-2738(92)90378-3.
[24] C. Weidlich, K.-M. Mangold, Electrochemically switchable polypyrrole coated membranes, Electrochim. Acta 56 (2011) 3481–3484, https://doi.org/10.1016/j.electacta.2010.11.065.
[25] S.M.A. Mokhtar, N. Nataren, D. Evans, M. Moore, S. Bradley, S. Palmar, et al., Molecular and histological evidence for the biocompatibility of PEDOT-coated microneedles in human skin, J. Mater. Chem. B 13 (2025), https://doi.org/10.1039/d4tb02281e.
[26] S.M.A. Mokhtar, A.L.K. Derrick-Roberts, D.R. Evans, X.L. Strudwick, Cell viability assessment of PEDOT conducting polymer-coated microneedles for skin sampling, ACS Appl. Bio Mater. 6 (2023) 4662–4671, https://doi.org/10.1021/acsabm.3c00416.
[27] J. Yu, R. Wan, F. Tian, J. Cao, W. Wang, Q. Liu, et al., 3D printing of robust high-performance conducting polymer hydrogel-based electrical bioadhesive interface for soft bioelectronics, Small 20 (2024) 2308778, https://doi.org/10.1002/smll.202308778.
[28] W. Li, Y. Li, Z. Song, Y.-X. Wang, W. Hu, PEDOT-based stretchable optoelectronic materials and devices for bioelectronic interfaces, Chem. Soc. Rev. 53 (2024) 10575–10603, https://doi.org/10.1039/D4CS00541D.
[29] K. Kontturi, L. Murtomäki, Impedance spectroscopy in human skin. A refined model, Pharm. Res. 11 (1994) 1355–1357, https://doi.org/10.1023/A:1018915100150.
[30] M.E. Orazem, N. Pébère, B. Tribollet, Enhanced graphical representation of electrochemical impedance data, J. Electrochem. Soc. 153 (2006), https://doi.org/10.1149/1.2168377. B129.
[31] S. Björklund, A. Nowacka, J.A. Bouwstra, E. Sparr, D. Topgaard, Characterization of stratum corneum molecular dynamics by natural-abundance ^{13}C solid-state NMR, PLoS One 8 (2013) e61889, https://doi.org/10.1371/journal.pone.0061889.
[32] S.Y. Oh, L. Leung, D. Bommannan, R.H. Guy, R.O. Potts, Effect of current, ionic strength and temperature on the electrical properties of skin, J. Contr. Release 27 (1993) 115–125, https://doi.org/10.1016/0168-3659(93)90215-Q.
[33] W.H.M. Craane-van Hinsberg, J.C. Verhoef, H.E. Junginger, H.E. Boddé, Thermoelectrical analysis of the human skin barrier, Thermochim. Acta 248 (1995) 303–318, https://doi.org/10.1016/0040-6031(94)01887-M.
[34] Y.N. Kalia, R.H. Guy, The electrical characteristics of human skin in vivo, Pharm. Res. 12 (1995) 1605–1613, https://doi.org/10.1023/A:1016228730522.
[35] J.D. DeNuzzio, B. Berner, Electrochemical and iontophoretic studies of human skin, J. Contr. Release 11 (1990) 105–112, https://doi.org/10.1016/0168-3659(90)90124-C.
[36] I. Nicander, M. Nyren, L. Emtestam, S. Ollmar, Baseline electrical impedance measurements at various skin sites - related to age and sex, Skin Res. Technol. 3 (1997) 252–258, https://doi.org/10.1111/j.1600-0846.1997.tb00194.x.
[37] S. Jankovskaja, J. Engblom, M. Rezeli, G. Marko-Varga, T. Ruzgas, S. Björklund, Non-invasive skin sampling of tryptophan/kynurenine ratio in vitro towards a skin cancer biomarker, Sci. Rep. 11 (2021) 678, https://doi.org/10.1038/s41598-020-79903-w.
[38] C. Albèr, B.D. Brandner, S. Björklund, P. Billsten, R.W. Corkery, J. Engblom, Effects of water gradients and use of urea on skin ultrastructure evaluated by confocal Raman microspectroscopy, Biochim. Biophys. Acta Biomembr. 1828 (2013) 2470–2478, https://doi.org/10.1016/j.bbamem.2013.06.011.
[39] M. Morin, T. Ruzgas, P. Svedenhag, C.D. Anderson, S. Ollmar, J. Engblom, et al., Skin hydration dynamics investigated by electrical impedance techniques in vivo and in vitro, Sci. Rep. 10 (2020) 17218, https://doi.org/10.1038/s41598-020-73684-y.
[40] Y. Itoh, A. Shimazu, Y. Sadzuka, T. Sonobe, S. Itai, Novel method for stratum corneum pore size determination using positron annihilation lifetime spectroscopy, Int. J. Pharm. 358 (2008) 91–95, https://doi.org/10.1016/j.ijpharm.2008.02.016.
[41] H. Tang, S. Mitragotri, D. Blankschtein, R. Langer, Theoretical description of transdermal transport of hydrophilic permeants: application to low-frequency sonophoresis, J. Pharmaceut. Sci. 90 (2001) 545–568, https://doi.org/10.1002/1520-6017(200105)90:5<545::AID-JPS1012>3.0.CO;2-H.
[42] D. Stein, M. Kruithof, C. Dekker, Surface-charge-governed ion transport in nanofluidic channels, Phys. Rev. Lett. 93 (2004) 035901, https://doi.org/10.1103/PhysRevLett.93.035901.
[43] Y. Itoh, A. Shimazu, Y. Sadzuka, T. Sonobe, S. Itai, Novel method for stratum corneum pore size determination using positron annihilation lifetime spectroscopy, Int. J. Pharm. 358 (2008) 91–95, https://doi.org/10.1016/j.ijpharm.2008.02.016.
[44] G.B. Kasting, M.A. Miller, T.D. LaCount, J. Jaworska, A composite model for the transport of hydrophilic and lipophilic compounds across the skin: steady-state behavior, J. Pharmaceut. Sci. 108 (2019) 337–349, https://doi.org/10.1016/j.xphs.2018.09.007.
[45] A. Fernández-Pumarega, B. Martín-Sanz, S. Amézqueta, E. Fuguet, M. Rosés, Estimation of the octanol-water distribution coefficient of basic compounds by a cationic microemulsion electrokinetic chromatography system, Admet dmpk 8 (2020) 98–112, https://doi.org/10.5599/admet.760.
[46] I. Hatta, Stratum corneum structure and function studied by X-ray diffraction, Dermato 2 (2022) 79–108, https://doi.org/10.3390/dermato2030009.
[47] J.A. Bouwstra, G.S. Gooris, W. Bras, D.T. Downing, Lipid organization in pig stratum corneum, J. Lipid Res. 36 (1995) 685–695.
[48] M.J. Hey, D.J. Taylor, W. Derbyshire, Water sorption by human cells, Biochim. Biophys. Acta Gen. Subj. 540 (1978) 518–533, https://doi.org/10.1016/0304-4165(78)90181-2.
[49] H. Nakazawa, N. Ohta, I. Hatta, A possible regulation mechanism of water content in human stratum corneum via intercellular lipid matrix, Chem. Phys. Lipids 165 (2012) 238–243, https://doi.org/10.1016/j.chemphyslip.2012.01.002.